Polymer Chemistry

ROYAL SOCIETY OF CHEMISTRY

PAPER

View Article Online
View Journal | View Issue

Cite this: *Polym. Chem.*, 2021, **12**, 3276

Polybenzoxazines: a sustainable platform for the design of fast responsive and catalyst-free vitrimers based on trans-esterification exchanges†

Antoine Adjaoud,[a,b] Acerina Trejo-Machin,[a,b] Laura Puchot[a] and Pierre Verge *[a]

This work explores a new strategy, aiming for the synthesis of catalyst-free vitrimers by taking advantage of the abundant number of tertiary amines covalently bound into a polybenzoxazine network. A bio-based monomer was obtained by reacting 4,4-bis(4-hydroxyphenyl)valeric acid, polyethylene glycol, paraformaldehyde and mono-ethanolamine, *via* consecutive solvent-free Fischer esterification and Mannich-like ring-closure. The two-step reaction led to the formation of quadri-telechelic benzoxazine-terminated polyethylene glycol monomers, containing ester bonds and aliphatic hydroxyl groups. The structural features of the resulting products were substantiated by ^{1}H NMR, ^{13}C NMR, elemental analysis, and FTIR. The occurrence of the thermally induced ring-opening polymerization was monitored by rheological measurements and DSC. At 140 °C, the monomers show a short gelation time (145 seconds). Once polymerized, the polybenzoxazine exhibits a relatively high temperature of α mechanical relaxation (93 °C). Due to the ability of tertiary amines to catalyze transesterification reactions, and to the abundant number of hydroxyl groups, the material enables exchange reactions without the use of an external catalyst. It possesses all the typical characteristics of a vitrimer, such as recycling, reshaping, and self-healing. Short stress-relaxation times were measured (116 s at 170 °C). Finally, the effect of the structural features of the vitrimer was investigated by tuning the crosslinking density of the network and the number of hydroxyl groups, shedding more light on the mechanism of self-catalysis and the range of properties. Therefore, such a strategy constitutes an efficient and versatile route for an easy elaboration of mono-component, catalyst-free, and fast responsive vitrimers.

Received 10th March 2021,
Accepted 7th April 2021

DOI: 10.1039/d1py00324k

rsc.li/polymers

1. Introduction

Over the past few decades, the apogee of industrialization has led to a compelling increase in the consumption of thermosets worldwide, resulting in an abundant source of wastes which cannot be recycled or repaired.[1] To address this issue, reversible dissociative or associative bonds have been inserted within the chemical structure of thermosets to create covalent adaptable networks (CANs), enabling self-healability or recyclability.[2–4] In 2011, Leibler and co-workers successfully introduced dynamic covalent bonds (DCBs) in thermoset polymer networks and developed the first "vitrimer", combining the antithetical properties of a thermoplastic and a thermoset.[5] At service temperatures, vitrimers behave like a traditional thermoset with high mechanical properties, chemical resistance, and insolubility. At higher temperatures, they display the fluidity and the reprocessing ability of a thermoplastic.[5–7]

The different strategies and methodologies conceived to design performant vitrimers can be found in the excellent reviews published by Du Prez *et al.*,[8–11] and Hillmyer and Dichtel.[12] Among these strategies, the dynamic transesterification reaction (TER) occurring between ester bonds and hydroxyl (–OH) groups has been reported as the most representative chemistry for driving vitrimer behaviors. In most cases, the TER requires the use of an external catalyst to trigger fast enough exchange reactions within a reasonable range of conditions. Numerous catalysts can be employed to control the transesterification reaction,[13] but solid or organic basic catalysts are preferred within a context of vitrimer material elaboration. Among them, zinc acetate ($Zn(OAc)_2$) is the most widely used, owing to its high efficiency.[5–7] Tertiary amine (NR_3) groups are also well-known sites of TER catalysis.[13–15] In one of their pioneering works, Leibler *et al.* evidenced that triazobi-

[a]*Luxembourg Institute of Science and Technology, Materials Research and Technology Department, 5 Avenue des Hauts-Fourneaux, L-4362 Esch-sur-Alzette, Luxembourg. E-mail: pierre.verge@list.lu*
[b]*University of Luxembourg, 2, Avenue de l'Université, L-4365 Esch-sur-Alzette, Luxembourg*

†Electronic supplementary information (ESI) available. See DOI: 10.1039/d1py00324k

cyclodecene (TBD), a bicyclic base containing a NR_3 group, gave similar results to $Zn(OAc)_2$.[5] Later, Williams *et al.*,[16] and more recently Zhang *et al.*,[17] have both demonstrated in elegant approaches that NR_3 covalently bound to the polymer network exert an internal catalysis on the transesterification reactions occurring in epoxy-acid systems. These studies join other recent research works dedicated to the development of internally catalyzed (or catalyst-free) vitrimers.[18–22] It is noteworthy that in the absence of a catalyst, the lifetime of a vitrimer relying on a transesterification mechanism could be greatly enhanced, particularly as the risk of ester hydrolysis would be reduced.[8] Thus, the elaboration of catalyst-free vitrimers appears of great importance, and the use of polymer structures containing tertiary amines seems to be a reasonable choice.

Polybenzoxazines (PBZs) are mono-component thermoset, polymers constituted of an abundant number of NR_3 coming from the auto-catalyzed ring-opening polymerization (ROP) of benzoxazines.[23] They are also a promising alternative to phenolic and epoxy resins thanks to their unique mechanical and thermal properties, such as a high glass transition temperature, near-zero shrinkage upon polymerization, and high char yield polymers.[24] Benzoxazine monomers are obtained from the condensation reaction of a phenolic compound, a primary amine and paraformaldehyde (PFA). For the past ten years, there has been an explosive growth of research works on polybenzoxazines, dedicated to the use of natural phenolic compounds and amines[25–43] as synthons of their monomers. As PFA can be synthesized from bio-ethanol or carbon dioxide, these precursors could be considered as 100% bio-based.[44] However, to solve the concern of its carcinogenetic, its substitution by more friendly aldehydes has been under the spotlight of very significant investigations.[45,46] It makes no doubts that polybenzoxazines with an excellent life cycle impact will emerge in the coming years.

As they are constituted from a permanent covalent network, PBZs suffer from similar drawbacks to traditional thermoset resins, and they cannot be recycled or reprocessed if they have not been specifically designed with this aim. Few works address this issue, mostly those written by Yagci and Kiskan.[47–49] Recently, Verge *et al.* developed the first vitrimer involving PBZs, showing recyclability, reshaping, and reversible adhesion properties.[50] The rearrangement of the permanent network was possible thanks to exchangeable disulfide bonds. However, to the best of our knowledge, none of the self-healable or reprocessable PBZs reported so far demonstrate vitrimer features from TER exchanges. Besides this, and more importantly, the NR_3 generated during the ROP of benzoxazines have never been considered as internal catalysts for TER exchanges.

Inspired by a bio-based PBZ we developed in the past,[51] and motivated by the outstanding achievements made on vitrimers over the past decade, this work attempts to illustrate how PBZs could be used to design catalyst-free vitrimers based on a transesterification mechanism. 4,4-Bis(4-hydroxyphenyl)valeric acid, more commonly known as diphenolic acid (DPA), is a bio-based diphenol coming from levulinic acid, a chemical extracted from lignocellulosic biomass.[52] DPA was used to esterify the end-chains of polyethylene glycol (PEG) to form a quadri-telechelic phenol-terminated PEG (PEG-DPA) containing ester bonds. Thus, the hydroxyphenyl moieties were reacted *via* a Mannich-like condensation with mono-ethanolamine (mea), an amine derived from L-serine, sorbitol or glycolaldehyde.[53,54] This reaction led to the formation of PEG-DPA-mea, a quadri-telechelic benzoxazine-terminated polyethylene glycol monomer with pending aliphatic –OH groups connected to the nitrogen atom (in β-position). These –OH groups were expected to transesterify with the ester bonds. The following paragraphs describe the synthesis of a series of bio-based material and the evidence that their vitrimer behavior does not require the use of an external catalyst. These materials fit many of the Green Chemistry and Engineering principles, such as "Use of renewable feedstocks", "Safer solvents and auxiliaries", "Durability rather than immortality", "Renewable rather than depleting", and "Design for Commercial after-life", to cite but a few.

2. Experimental section

2.1 Materials and chemicals

4,4-Bis(4-hydroxyphenyl)valeric acid (95%, diphenolic acid, DPA), polyethylene glycol (average M_n = 200, 400 and 2000 g mol^{-1}; PEG_{200}, PEG_{400}, PEG_{2000}), mono-ethanolamine (≥98%, mea), furfurylamine (≥99%, fa) paraformaldehyde (95%, PFA), and *para*-toluene sulfonic acid monohydrate (≥98.5%, *p*-TSA) were purchased from Sigma-Aldrich. All chemicals were reagent grade and used as received without any further purification.

2.2 Equipment and characterizations

Nuclear Magnetic Resonance (NMR) spectroscopy was performed on an AVANCE III HD Bruker spectrometer equipped with a 5 mm BBO-probe operating at a proton frequency of 600 MHz. All chemical shifts are given as δ value (ppm) referenced to tetramethylsilane (TMS) as an internal standard. Assignments were performed using a combination of COSY, HSQC, and HMBC spectra. Methyl peak ($-CH_3$) in α-position of the aromatic ring was used as the reference for the integration of all other peaks (6.00H). Peak multiplicity was indicated as follows: singlet (s); doublet (d); triplet (t) or multiplet (m). The coupling constants (J) were reported in Hertz (Hz).

Fourier transform infrared spectroscopy (FTIR) was conducted on a Bruker TENSOR 27 instrument in the attenuated total reflection (ATR) mode using a diamond crystal. All spectra were recorded at room temperature in direct absorbance mode across 4000–400 cm^{-1} frequency range (32 scans, 4 cm^{-1} spectral resolution).

Elemental analysis (CHNS measurements) was performed on a Vario MACRO cube CHNS/O from Elementar France

SARL. Samples were put into an oxygen-enriched furnace at 1150 °C, where a combustion process converted carbon-to-carbon dioxide; hydrogen to water; nitrogen-to-nitrogen gas/oxides of nitrogen and sulfur-to-sulfur dioxide. The combustion products were swept out of the combustion chamber by an inert carrier gas (He, 600 mL min^{-1}) and passed over heated (850 °C) high purity copper. The separation of the measuring components took place as follows: nitrogen (N_2) was not adsorbed in the adsorption columns and was the first measuring component to enter the thermal conductivity detector directly. The other components were adsorbed in their respective adsorption column. Each of these columns was then heated separately to the corresponding desorption temperature ($T_{desorpt.}$) in order to release the components in the following order: CO_2 ($T_{desorpt.}$ = 240 °C), H_2O ($T_{desorpt.}$ = 150 °C) and SO_2 ($T_{desorpt.}$ = 100 °C or 230 °C). After desorption, each component was transported by the carrier gas flow into the measuring cell of a thermal conductivity detector (TCD).

Differential scanning calorimetry (DSC) thermograms were recorded on a Netzsch DSC 204 F1 Phoenix device in standard pierced aluminum crucibles (40 μL). A linear heating ramp from −25 to 300 °C at 10 °C min^{-1} rate was applied under inert atmosphere (N_2). The DSC thermogram of the PBZ material was recorded over two consecutive heating–cooling cycles from −25 to 250 °C (heating rate of 10 °C min^{-1} and cooling rate of 20 °C min^{-1}) to determine the glass transition (T_g) of the polymer and to ensure complete polymerization.

Thermogravimetric analysis (TGA) was completed on the Mettler Toledo TGA 2 device in standard ceramic alumina pan from 25 to 800 °C at 10 °C min^{-1} rate under air or inert atmosphere (N_2). The maximum of the degradation temperature was determined using the derivative of the TGA curve (DTG).

Rheological measurements were recorded using an Anton Paar Physica MCR 302 rheometer equipped with a CTD 450 temperature control device. Stress relaxation experiments were performed on disk-shaped solid geometry with a disposable aluminum plate–plate (ϕ = 25 mm). The relaxation modulus was followed as a function of time for 2000 s between 120 °C and 170 °C with a constant applied strain of 1% and normal force of 20 N. The original relaxation modulus (G_0) was extracted from the initial plateau of the stress relaxation curves (onset point of the second derivative curve). For the isothermal rheo-kinetic measurements, small quantities of the samples were loaded in a parallel plate-plate geometry (ϕ = 25 mm). The polymerization measurements were recorded in the oscillation mode at a frequency of 1 Hz and a controlled strain of 0.1%. Heating ramps of 20 °C min^{-1} were applied to reach a temperature of 140 °C. The sample deformation was ramped linearly from 1% to 0.2% to remain within the instrument's limitation and to maintain a linear viscoelastic behavior as the moduli (G' storage modulus, G'' loss modulus) increase by several orders of magnitude upon curing. The gap between the plates was maintained at 0.5 mm during all the experiments. Rheology temperature sweep curves were performed on the bar-shaped solid in rectangular-torsion mode under constant deformation of 0.1% (1 Hz).

Dilatometry thermogram was recorded on the Netzsch DIL 402 C apparatus from 25 to 200 °C (2 °C min^{-1}) under an inert atmosphere (N_2) and a constant force to avoid buckling (30 cN). The material was introduced in a hollow cylinder capped at the extremities by two solid cylindrical end pieces to limit the side expansion.

Dynamic mechanical analysis (DMA) was used to evaluate the mechanical properties of the material after reprocessing. The cured and reprocessed materials were analyzed at room temperature (RT) in tension and in single cantilever mode (effective lengths of 10 and 5 mm, respectively, width 5 mm, thickness 1.25 mm). The measurements were performed at 1 Hz using a preload force of 0.05 N and a sinusoidal strain of 10 μm. The storage modulus (E') was recorded as a function of time. The reported values are an average of three values.

Optical microscopy was used to illustrate the self-healing performance of the PBZ vitrimer. The surface morphology of scratched samples was examined using the Nikon Universal Design Microscope UDM ECLIPSE LV100D-U (optics ×20, gain ×2.40, exposure 6 ms). The healing process was conducted at 150 °C in a convection oven. The width of the crack was measured before and after the healing process in a dynamic contrast mode at different time intervals.

Swelling experiments were conducted in acetone, chloroform and water by immersion at room temperature of 25 mg of the material in 2 mL of solvent at different time intervals for poly(PEG_{400}-DPA-mea). The crosslinking density was measured by swelling tests in water at different time intervals. The swelling ratio (W) is determined according to the eqn (1):

$$W = \frac{m_s - m_i}{m_i} \quad (1)$$

with m_i and m_s being the initial and the swollen mass, respectively. The molecular weight between the crosslinking nodes ($\overline{M_c}$) was calculated by applying the Flory Rehner equation (2):

$$\overline{M_c} = \frac{\rho \times V \times (0.5 \times \mu - \mu^{\frac{1}{3}})}{\ln(1-\mu) + \mu + \chi_{PEG/water} \times \mu^2} \quad (2)$$

where ρ is the density of the polymer, V is the molar volume of water, μ is the polymer volume fraction in the equilibrium-swollen system and $\chi_{PEG/water}$ is the interaction parameter of PEG with water. We took the hypothesis that PEG moieties were driving the interaction of the network with water and $\chi_{PEG/water}$ approximated to 0.5.[55] μ is determined according to the eqn (3):

$$\mu = \left[1 + W \times \frac{d_{polymer}}{d_{solvent}}\right]^{-1} \quad (3)$$

where $d_{polymer}$ and $d_{solvent}$ are the density of the polybenzoxazine vitrimer and the water, respectively. The crosslinking density (ν_c) is calculated according the eqn (4):

$$\nu_c = \frac{d_{polymer}}{M_c} \quad (4)$$

2.3 Synthetic procedure

2.3.1 Synthesis of PEG$_n$-DPA. Diphenol terminated polyethylene glycols (PEG$_n$-DPA) were synthesized *via* a Fischer esterification, from a previous work with minor modification.[51] Three PEG of different molecular weight (200, 400 or 2000 g mol^{-1}) were used for the synthesis. Typically, PEG$_n$ (1.0 eq.) was reacted with DPA (2.0 eq.) and *p*-TSA (0.5 wt%) in an open three-neck round bottom flask at 130 °C for 24 hours under mechanical stirring (Ministar 20 Digital, anchor stirrer, 200 rpm). The reaction crude was then solubilized in butanone and purified by three liquid–liquid extractions with distilled water to remove non-hydrolyzed *p*-TSA. The solvent was then evaporated under reduced pressure. Finally, the product was dried overnight under reduced pressure (<1 mBar) at T = 50 °C.

PEG$_{200}$-DPA (brown powder). ^{1}H NMR (DMSO-d$_6$, 600 MHz, 298°K): δ (ppm) = (assignment, multiplicity (coupling constant), [attribution], experimental integration, theoretical integration). δ = 1.46 (C–CH$_3$*, s, [c], exp 6.00H, th 6.00H); δ = 2.02 (CH$_2$–CH$_2$*–C═O, t (J = 6.91 Hz), [a], exp 3.98H, th 4.00H); δ = 2.24 (C–CH$_2$*–CH$_2$, t (J = 7.37 Hz), [b], exp 3.97H, th 4.00H); δ = 3.48 (O–CH$_2$*, t (J = 3.66 Hz), [3], exp 9.01H); δ = 3.55 (O═C–O–CH$_2$-βCH2*, m, [1], exp 4.04H, th 4.00H); δ = 4.06 (O═C–O-αCH$_2$*–CH$_2$, t, [2], exp 3.78H, th 4.00H); δ = 6.65 (C═CH*–CH, d (J = 8.56 Hz), [e], exp 8.00H, th 8.00H); δ = 6.93 (CH–CH*═C–O, d (J = 8.44 Hz), [d], exp 8.00H, th 8.00H); δ = 9.18 (Ar–OH*, s, [f], exp 3.99H, th 4.00H).

^{13}C NMR (DMSO-d$_6$, 600 MHz, 298°K): δ (ppm) = 27.7 [e]; 30.3 [b]; 36.7 [c]; 44.3 [d]; 63.6 [2]; 68.7 [1]; 70.2 [3]; 115.2 [h]; 128.2 [g]; 139.7 [f]; 155.5 [i]; 173.5 [a].

PEG$_{400}$-DPA (brown viscous substance). ^{1}H NMR (DMSO-d$_6$, 600 MHz, 298°K): δ (ppm) = (assignment, multiplicity (coupling constant), [attribution], experimental integration, theoretical integration). δ = 1.44 (C–CH$_3$*, s, [c], exp 6.00H, th 6.00H); δ = 2.03 (CH$_2$–CH$_2$*–C═O, t (J = 7.90 Hz), [a], exp 4.00H, th 4.00H); δ = 2.24 (C–CH$_2$*–CH$_2$, t (J = 7.93 Hz), [b], exp 3.99H, th 4.00H); δ = 3.48 (O–CH$_2$*, t (J = 2.78 Hz), [3], exp 30.3H); δ = 3.55 (O═C–O–CH$_2$-βCH2*, m, [1], exp 4.13H, th 4.00H); δ = 4.06 (O═C–O-αCH$_2$*–CH$_2$, t, [2], exp 3.98H, th 4.00H); δ = 6.65 (C═CH*–CH, d (J = 8.57 Hz), [e], exp 8.02H, th 8.00H); δ = 6.93 (CH–CH*═C–O, d (J = 8.53 Hz), [d], exp 7.98H, th 8.00H); δ = 9.19 (Ar–OH*, s, [f], exp 4.02H, th 4.00H).

^{13}C NMR (DMSO-d$_6$, 600 MHz, 298°K): δ (ppm) = 27.7 [e]; 30.3 [b]; 36.7 [c]; 44.3 [d]; 63.6 [2]; 68.7 [1]; 70.2 [3]; 115.1 [h]; 128.2 [g]; 139.6 [f]; 155.5 [i]; 173.5 [a].

FTIR (cm^{-1}); very strong (vs), strong (s), medium (m), weak (w), broad (br): 3339 (–OH stretching, br), 2869 (C–H stretching, vs), 1730 (C═O stretching from the ester, s), 1625–1475 (C═C stretching vibrations from the aromatic ring, m), 1175 (phenol C–O stretching and –OH in plane deformation, w), 1083 (C–O stretching from the ester, s).

PEG$_{2000}$-DPA (brown wax). ^{1}H NMR (DMSO-d$_6$, 600 MHz, 298°K): δ (ppm) = (assignment, multiplicity (coupling constant), [attribution], experimental integration, theoretical integration). δ = 1.46 (C–CH$_3$*, s, [c], exp 6.00H, th 6.00H); δ = 2.03 (CH$_2$–CH$_2$*–C═O, t (J = 8.04 Hz), [a], exp 4.11H, th 4.00H); δ = 2.24 (C–CH$_2$*–CH$_2$, t (J = 8.12 Hz), [b], exp 4.00H, th 4.00H); δ = 3.51 (O–CH$_2$*&O═C–O–CH$_2$-βCH2*, [3,1], exp 191.14H); δ = 4.06 (O═C–O-αCH$_2$*–CH$_2$, t, [2], exp 4.00H, th 4.00H); δ = 6.65 (C═CH*–CH, d (J = 8.61 Hz), [e], exp 7.95H, th 8.00H); δ = 6.93 (CH–CH*═C–O, d (J = 8.61 Hz), [d], exp 7.96H, th 8.00H); δ = 9.18 (Ar–OH*, s, [f], exp 4.07H, th 4.00H).

^{13}C NMR (DMSO-d$_6$, 600 MHz, 298°K): δ (ppm) = 27.7 [e]; 30.3 [b]; 36.7 [c]; 44.3 [d]; 63.6 [2]; 68.7 [1]; 70.2 [3]; 115.1 [h]; 128.2 [g]; 139.6 [f]; 155.5 [i]; 173.5 [a].

2.3.2 Synthesis of PEG$_n$-DPA-mea. Freshly prepared diphenol-terminated polyethylene glycol (PEG$_n$-DPA, 1.0 eq.) was reacted solventless with mea (4.0 eq.) and PFA (8.0 eq.) at 85 °C for 2.5 hours followed by 0.5 hours at 90 °C under mechanical stirring (Ministar 20 Digital, anchor stirrer, 200 rpm). PEG$_n$-DPA-mea benzoxazine monomers were all used without any purification.

PEG$_{200}$-DPA-mea (yellow powder). ^{1}H NMR (DMSO-d$_6$, 600 MHz, 298 K): δ (ppm) = (assignment, multiplicity (coupling constant), [attribution], experimental integration, theoretical integration). δ = 1.47 (C–CH$_3$*, s, [c], exp 6.00H, th 6.00H); δ = 2.03 (CH$_2$–CH$_2$*–C═O, m, [a], exp 3.97H, th 4.00H); δ = 2.25 (C–CH$_2$*–CH$_2$, m, [b], exp 3.87H, th 4.00H); δ = 2.71 (N–CH$_2$*–CH$_2$, m, [i], exp 6.06H, th 8.00H); δ = 3.48 (O–CH$_2$*, m, [3], exp 11.01H); δ = 3.55 (CH$_2$–CH$_2$*–OH & O═C–O–CH$_2$-βCH$_2$*, m, [1, j], exp 10.60H, th 12.00H); δ = 3.91 (Ar–CH$_2$*–N, s, [h], exp 5.30H, th 8.00H); δ = 4.05 (O═C–O-αCH$_2$*–CH$_2$, m, [2], exp 3.98H, th 4.00H); δ = 4.52 (CH$_2$–OH*, s, [k], exp 3.34H, th 4.00H); δ = 4.78 (O–CH$_2$*–N, s, [g], exp 5.62H, th 8.00H); δ = 6.82 (C═CH*–CH & C═CH*–C & CH–CH*═C–O, m, [d, f, e], exp 11.78, th 12.00H).

^{13}C NMR (DMSO-d$_6$, 600 MHz, 298 K): δ (ppm) = 27.5 [e]; 30.3 [b]; 36.5 [c]; 44.5 [d]; 50.6 [m]; 54.0 [n]; 60.0 [o]; 63.6 [2]; 68.7 [1]; 70.2 [3]; 83.1 [l]; 115.9 [i]; 120.3 [k]; 126.0 [g]; 126.6 [h]; 140.8 [f]; 152.3 [j]; 173.5 [a].

PEG$_{400}$-DPA-mea (orange viscous substance). ^{1}H NMR (DMSO-d$_6$, 600 MHz, 298 K): δ (ppm) = (assignment, multiplicity (coupling constant), [attribution], experimental integration, theoretical integration). δ = 1.45 (C–CH$_3$*, s, [c], exp 6.00H, th 6.00H); δ = 2.02 (CH$_2$–CH$_2$*–C═O, m, [a], exp 4.03H, th 4.00H); δ = 2.29 (C–CH$_2$*–CH$_2$, m, [b], exp 4.05H, th 4.00H); δ = 2.72 (N–CH$_2$*–CH$_2$, m, [i], exp 5.92H, th 8.00H); δ = 3.48 (O–CH$_2$*, m, [3], exp 30.68H); δ = 3.55 (CH$_2$–CH$_2$*–OH & O═C–O–CH$_2$-βCH$_2$*, m, [1, j], exp 10.20H, th 12.00H); δ = 3.88 (Ar–CH$_2$*–N, s, [h], exp 5.96H, th 8.00H); δ = 4.06 (O═C–O-αCH$_2$*–CH$_2$, m, [2], exp 3.99H, th 4.00H); δ = 4.51 (CH$_2$–OH*, s, [k], exp 3.88H, th 4.00H); δ = 4.80 (O–CH$_2$*–N, s, [g], exp 5.93H, th 8.00H); δ = 6.81 (C═CH*–CH & C═CH*–C & CH–CH*═C–O, m, [d, f, e], exp 12.07, th 12.00H).

^{13}C NMR (DMSO-d$_6$, 600 MHz, 298 K): δ (ppm) = 27.5 [e]; 30.3 [b]; 36.5 [c]; 44.5 [d]; 50.6 [m]; 54.0 [n]; 60.0 [o]; 63.7 [2];

68.7 [1]; 70.2 [3]; 83.1 [l]; 116.0 [i]; 120.3 [k]; 126.0 [g]; 126.6 [h]; 140.8 [f]; 152.3 [j]; 173.5 [a].

FTIR (cm^{-1}); very strong (vs), strong (s), medium (m), weak (w), broad (br): 3339 (–OH stretching, br), 2869 (C–H stretching, vs), 1730 (C=O stretching from the ester, s), 1625–1475 (C=C stretching vibrations from the aromatic ring, m), 1230 (C–O–C oxazine asymmetric stretching, m), 1083 (C–O stretching from the ester, s), 1030 (primary alcohol C–O stretching and –OH in plane deformation, w), 928 (C–H out-of-plane vibration in the trisubstituted benzene ring, m).

Elemental analysis (exp, th): C (67, 68), H (150, 98), N (4, 4), S (<0.05, 0).

PEG_{2000}-DPA-mea (yellowish wax). ^{1}H NMR (DMSO-d_6, 600 MHz, 298 K): δ (ppm) = (assignment, multiplicity (coupling constant), [attribution], experimental integration, theoretical integration). δ = 1.47 (C–CH_3*, s, [c], exp 6.00H, th 6.00H); δ = 2.04 (CH_2–CH_2*–C=O, m, [a], exp 3.81H, th 4.00H); δ = 2.26 (C–CH_2*–CH_2, m, [b], exp 4.00H, th 4.00H); δ = 2.72 (N–CH_2*–CH_2, m, [i], exp 5.44H, th 8.00H); δ = 3.51 (O–CH_2*& CH_2–CH_2*–OH & O=C–O–CH_2-βCH_2*, m, [3, 1, j], exp 197.19H); δ = 3.92 (Ar–CH_2*–N, s, [h], exp 5.61H, th 8.00H); δ = 4.07 (O=C–O-αCH_2*–CH_2, m, [2], exp 4.06H, th 4.00H); δ = 4.52 (CH_2–OH*, s, [k], exp 3.86H, th 4.00H); δ = 4.78 (O–CH_2*–N, s, [g], exp 5.41H, th 8.00H); δ = 6.83 (C=CH*–CH & C=CH*–C & CH–CH*=C–O, m, [d, f, e], exp 12.97, th 12.00H).

^{13}C NMR (DMSO-d_6, 600 MHz, 298 K): δ (ppm) = 27.6 [e]; 30.3 [b]; 36.6 [c]; 44.5 [d]; 50.6 [m]; 54.0 [n]; 60.0 [o]; 63.7 [2]; 68.7 [1]; 70.3 [3]; 83.1 [l]; 115.9 [i]; 120.3 [k]; 126.0 [g]; 126.6 [h]; 140.8 [f]; 152.3 [j]; 173.5 [a].

2.3.3 Synthesis of PEG_{400}-DPA-mea_x/fa_{100-x}. Typically, freshly prepared diphenol-terminated polyethylene glycol (PEG_{400}-DPA, 1.0 eq.) was reacted solventless with a mixture of mea ((x/100) × 4.0 eq.) and fa (((100 − x)/100) × 4.0 eq.), and PFA (8.0 eq.) at 70 °C for 36 hours under mechanical stirring (Ministar 20 Digital, anchor stirrer, 200 rpm). PEG_{400}-DPA-mea_x/fa_{100-x} benzoxazine monomers were all used without any purification (orange viscous solid).

PEG_{400}-DPA-mea_{75}/fa_{25}. ^{1}H NMR (DMSO-d_6, 600 MHz, 298 K): δ (ppm) = (assignment, multiplicity (coupling constant), [attribution], experimental integration, theoretical integration). δ = 1.46 (C–CH_3*, s, [c], exp 6.00H, th 6.00H); δ = 2.04 (CH_2–CH_2*–C=O, m, [a], exp 3.89H, th 4.00H); δ = 2.26 (C–CH_2*–CH_2, m, [b], exp 3.99H, th 4.00H); δ = 2.72 (N–CH_2*–CH_2, m, [i], exp 4.73H, th 6.00H); δ = 3.49 (O–CH_2*, m, [3], exp 32.49H); δ = 3.55 (CH_2–CH_2*–OH & O=C–O–CH_2-βCH_2*, m, [1, j], exp 8.88H, th 10.00H); δ = 3.90 (*fa*-CH_2*–N & Ar–CH_2*–N, s, [l, h], exp 7.43H, th 10.00H); δ = 4.07 (O=C–O-αCH_2*-CH_2, m, [2], exp 4.01H, th 4.00H); δ = 4.51 (CH_2–OH*, s, [k], exp 2.75H, th 3.00H); δ = 4.78 (O–CH_2*–N, s, [g], exp 5.77H, th 8.00H); δ = 6.30 (*fa*-C=CH*–CH, s, [m], exp 0.91H, th 1.00H); δ = 6.41 (*fa*-CH–CH*=CH, s, [n], exp 0.92H, th 1.00H); δ = 6.82 (C=CH*–CH & C=CH*–C & CH–CH*=C–O, m, [d, f, e], exp 11.96, th 12.00H); δ = 7.60 (*fa*-CH=CH*–O, s, [o], exp 0.91H, th 1.00H).

^{13}C NMR (DMSO-d_6, 600 MHz, 298 K): δ (ppm) = 27.6 [e]; 30.3 [b]; 36.5 [c]; 44.5 [d]; 48.0 [p]; 49.6 [m_{fa}]; 50.6 [m_{mea}]; 54.0 [n]; 60.0 [o]; 63.7 [2]; 68.7 [1]; 70.3 [3]; 81.8 [l_{fa}]; 83.1 [l_{mea}]; 109.1 [r]; 110.9 [s]; 115.9 [i]; 119.6 [k_{fa}]; 120.3 [k_{mea}]; 126.0 [g]; 126.6 [h]; 140.8 [f]; 143.1 [t]; 152.3 [j&q]; 173.5 [a].

PEG_{400}-DPA-mea_{50}/fa_{50}. ^{1}H NMR (DMSO-d_6, 600 MHz, 298 K): δ (ppm) = (assignment, multiplicity (coupling constant), [attribution], experimental integration, theoretical integration). δ = 1.48 (C–CH_3*, s, [c], exp 6.00H, th 6.00H); δ = 2.05 (CH_2–CH_2*–C=O, m, [a], exp 3.94H, th 4.00H); δ = 2.27 (C–CH_2*–CH_2, m, [b], exp 3.96H, th 4.00H); δ = 2.72 (N–CH_2*–CH_2, m, [i], exp 3.05H, th 4.00H); δ = 3.49 (O–CH_2*, m, [3], exp 31.12H); δ = 3.55 (CH_2–CH_2*–OH & O=C–O–CH_2-βCH_2*, m, [1, j], exp 7.32H, th 8.00H); δ = 3.90 (*fa*-CH_2*–N & Ar–CH_2*–N, s, [l, h], exp 9.58H, th 12.00H); δ = 4.07 (O=C–O-αCH_2*–CH_2, m, [2], exp 4.00H, th 4.00H); δ = 4.52 (CH_2–OH*, s, [k], exp 1.81H, th 2.00H); δ = 4.78 (O–CH_2*–N, s, [g], exp 6.10H, th 8.00H); δ = 6.29 (*fa*-C=CH*–CH, s, [m], exp 1.78H, th 2.00H); δ = 6.40 (*fa*-CH–CH*=CH, s, [n], exp 1.89H, th 2.00H); δ = 6.84 (C=CH*–CH & C=CH*–C & CH–CH*=C–O, m, [d, f, e], exp 11.91, th 12.00H); δ = 7.59 (*fa*-CH=CH*–O, s, [o], exp 1.87H, th 2.00H).

^{13}C NMR (DMSO-d_6, 600 MHz, 298 K): δ (ppm) = 27.5 [e]; 30.3 [b]; 36.5 [c]; 44.5 [d]; 48.0 [p]; 49.6 [m_{fa}]; 50.6 [m_{mea}]; 54.0 [n]; 60.0 [o]; 63.7 [2]; 68.7 [1]; 70.2 [3]; 81.8 [l_{fa}]; 83.1 [l_{mea}]; 109.1 [r]; 110.9 [s]; 115.9 [i]; 119.6 [k_{fa}]; 120.3 [k_{mea}]; 126.0 [g]; 126.6 [h]; 140.8 [f]; 143.1 [t]; 152.3 [j&q]; 173.5 [a].

PEG_{400}-DPA-mea_{25}/fa_{75}. ^{1}H NMR (DMSO-d_6, 600 MHz, 298 K): δ (ppm) = (assignment, multiplicity (coupling constant), [attribution], experimental integration, theoretical integration). δ = 1.48 (C–CH_3*, s, [c], exp 6.00H, th 6.00H); δ = 2.05 (CH_2–CH_2*–C=O, m, [a], exp 4.00H, th 4.00H); δ = 2.27 (C–CH_2*–CH_2, m, [b], exp 3.97H, th 4.00H); δ = 2.72 (N–CH_2*–CH_2, m, [i], exp 1.55H, th 2.00H); δ = 3.49 (O–CH_2*, m, [3], exp 31.38H); δ = 3.56 (CH_2–CH_2*–OH & O=C–O–CH_2-βCH_2*, m, [1, j], exp 6.09H, th 6.00H); δ = 3.89 (*fa*-CH_2*–N & Ar–CH_2*–N, s, [l, h], exp 10.79H, th 14.00H); δ = 4.07 (O=C–O-αCH_2*–CH_2, m, [2], exp 3.94H, th 4.00H); δ = 4.51 (CH_2–OH*, s, [k], exp 1.01H, th 1.00H); δ = 4.78 (O–CH_2*–N, s, [g], exp 5.82H, th 8.00H); δ = 6.29 (*fa*-C=CH*–CH, s, [m], exp 2.71H, th 3.00H); δ = 6.40 (*fa*-CH–CH*=CH, s, [n], exp 2.73H, th 3.00H); δ = 6.84 (C=CH*–CH & C=CH*–C & CH–CH*=C–O, m, [d, f, e], exp 11.99, th 12.00H); δ = 7.69 (*fa*-CH=CH*–O, s, [o], exp 2.80H, th 3.00H).

^{13}C NMR (DMSO-d_6, 600 MHz, 298 K): δ (ppm) = 27.5 [e]; 30.3 [b]; 36.5 [c]; 44.5 [d]; 48.0 [p]; 49.6 [m_{fa}]; 50.6 [m_{mea}]; 54.0 [n]; 60.0 [o]; 63.7 [2]; 68.7 [1]; 70.2 [3]; 81.8 [l_{fa}]; 83.1 [l_{mea}]; 109.1 [r]; 110.8 [s]; 116.0 [i]; 119.6 [k_{fa}]; 120.3 [k_{mea}]; 126.2 [g]; 126.8 [h]; 141.1 [f]; 143.1 [t]; 152.3 [j&q]; 173.5 [a].

2.3.3 Elaboration of the polybenzoxazine vitrimer: poly (PEG_n-DPA-mea_x/fa_{100-x}). The benzoxazine monomer was placed in a hollow Teflon® mold (70 × 20 × 0.3 mm). The mold was covered with a Kapton® polyimide film to ensure homogeneous and smooth surfaces. The mold was placed in a vacuum chamber and heated for one hour at 100 °C to remove traces of water (that could lead to bubbles inside the final material) and allow the monomer to flow in the mold. The mold was then transferred to an air-circulating oven at 150 °C for one hour for the curing step (speed fan of 30%). For poly (PEG_{400}-DPA-mea_x/fa_{100-x}), an additional post-curing step (170 °C for half an hour) was performed to ensure the com-

plete polymerization. The polymeric material was cooled to RT before testing. Starting from a disc or a bar-shaped mold, diverse material shapes, suitable for mechanical and vitrimer characterization, were achieved.

2.3.4 Reshaping and reprocessing of poly(PEG_{400}-DPA-mea). The original material was reshaped after heating above 100 °C for at least two minutes (heat gun). For the reprocessing, the cured material was firstly dipped in a liquid N_2 bath for a couple of minutes. The hardened polymeric material was ground to a fine powder using Retsch Ultra Centrifugal Mill ZM 200 apparatus (6000 rpm, ϕ < 40 μm). The powder was poured into a disc-shaped brass mold sandwiched between two steel plates covered by Teflon® and paper hot-pressed for one hour at 150 °C under low pressure (<10 Pa). The reprocessed PBZ was then removed from the mold and cooled to RT before testing.

3. Results and discussion

For the sake of clarity, the first part of the discussion is focusing on the synthesis and the characterization of PEG_{400}-DPA-mea. All the materials discussed later in this manuscript (subsection 3.2.2) have been prepared and characterized following the same procedures, detailed in the ESI.†

3.1 Synthesis and characterization of the vitrimer precursors

PEG_{400}-DPA-mea was synthesized solventless in two steps (Scheme 1), following a procedure previously reported by our group.[51] The phenolation of polyethylene glycol 400 (PEG_{400}) *via* a Fischer esterification was realized with diphenolic acid (DPA), with *p*-toluene sulfonic acid as the catalyst (*p*-TSA), and led to the formation of a quadri-telechelic phenol terminated PEG (PEG_{400}-DPA). It is noteworthy that PEG_{400} was specifically considered for the synthesis of the benzoxazine monomers because its industrial production adheres to many of the principles of the Green Chemistry.[56] PEG_{400}-DPA was purified by liquid–liquid extractions to remove non-hydrolyzed *p*-TSA. PEG_{400}-DPA was then reacted with mono-ethanolamine (mea) and paraformaldehyde (PFA) *via* Mannich-like condensation followed by a ring-closure process. Mea was purposely used to cap the extremities of the monomer with pending –OH groups, which are able to react further by transesterification with the ester bonds of the PEG_{400}-DPA backbone. In fine, a quadri-telechelic benzoxazine-terminated PEG monomer was obtained (PEG_{400}-DPA-mea). It is noteworthy that this second step, *i.e.* Mannich-like condensation with an amino-alcohol, may compete with various detrimental side reactions when performed in a solvent, leading to the formation of hydroxybenzylaminoethanol, oxazolidine, triazacyclohexane, or diazaheptane derivatives (depending on the initial molar ratio).[57,58] To sidestep these competing reactions, the Mannich condensation was performed in various conditions (Table S1†). The highest conversion yields of phenolic counterparts into oxazine rings were obtained when the synthesis was performed in the absence of solvents and below 100 °C.

The structural features of PEG_{400}-DPA and PEG_{400}-DPA-mea were characterized by ^{1}H NMR, ^{13}C NMR, FTIR and elemental analysis (Fig. 1, Fig. S1–3†). The ^{1}H NMR spectrum of PEG_{400}-DPA (Fig. 1a) reveals peaks corresponding to methylene protons [1,2] adjacent to the carbonyl group in β- and α-position (δ = 3.55 and = 4.06 ppm respectively), attesting the successful esterification of PEG_{400}. Furthermore, the characteristic carbonyl peak [a] at δ = 173.5 ppm in ^{13}C NMR (Fig. S1†) and its correlation in 2D NMR with DPA characteristic methylene protons [1,2] confirm the formation of the ester bond. The absence of impurities or by-products peaks suggests that quantitative conversion was nearly reached. From the ^{1}H NMR spectrum of PEG_{400}-DPA-mea (Fig. 1b), the characteristic peaks corresponding to the formation of the benzoxazine rings are revealed at δ = 3.88 and δ = 4.80 ppm, which correspond to Ar–CH_2*–N [h] and O–CH_2*–N [g], respectively. The experimental integrations of the methylene protons of the oxazine rings are 5.81H and 5.95H, respectively, corresponding to roughly 75% of the closed benzoxazine rings (theoretical value of 8.00H each). The remaining 25% of end-capping is attributed to opened benzoxazine rings labelled with * in Fig. 1b. In such opened structures, the primary amine has reacted with the phenolic group, but the ring is not closed between the –OH and the nitrogen. The non-closed structures can still be involved in the crosslinking process and affect the rate of transesterification reactions similarly to closed structures. The disappearance of the peak at δ = 9.2 ppm suggests that 100% of the phenolic groups reacted, and this is confirmed by elemental analysis as the experimental ratio of carbon and nitrogen atoms C/N is equal to 67/4 (theoretical C/N = 68/4). The wide signal centered at δ = 4.51 ppm is attributed to the aliphatic hydroxyl groups –OH [k] (ex. 3.88H, th 4.00H). In the ^{13}C NMR spectrum (Fig. S2†), the characteristic oxazine ring carbons are found at δ = 50.6 and δ = 83.1 ppm (for Ar–*CH_2–N [m] and O–*CH_2–N [l], respectively). The formation of PEG_{400}-DPA-mea was also confirmed by FTIR analysis (Fig. S3†). The strong absorption peak at 1730 cm^{-1} is typical of the ester C=O stretching. The presence of the benzoxazine rings, confirmed by the characteristic bands at 1230 and 932 cm^{-1} (attributed to the C–O–C asymmetric stretching and the C–H out-of-plane vibration in the trisubstituted benzene ring, respectively), and by the decrease of the intensity of the –OH stretching vibration centered at 3339 cm^{-1}. Finally, the peak at 1030 cm^{-1} corresponds to the absorption of the primary alcohol C–O stretching and –OH in-plane deformation.

DSC measurements revealed that PEG_{400}-DPA and PEG_{400}-DPA-mea have a similar softening temperature (5.6 and 7.2 °C respectively, Fig. S4†). An exothermic peak ($T_{exo,1}$ = 110–220 °C) was observed only in the case of PEG_{400}-DPA-mea, attributed to the ring-opening polymerization (ROP) of benzoxazine moieties. It is worth indicating the benzoxazine ROP is triggered at a very low temperature compared to traditional benzoxazines, generally in the range of 150–200 °C.[59] The apparent low ROP temperature is related to the activating effect of alcohol functionality through hydrogen bonding, as

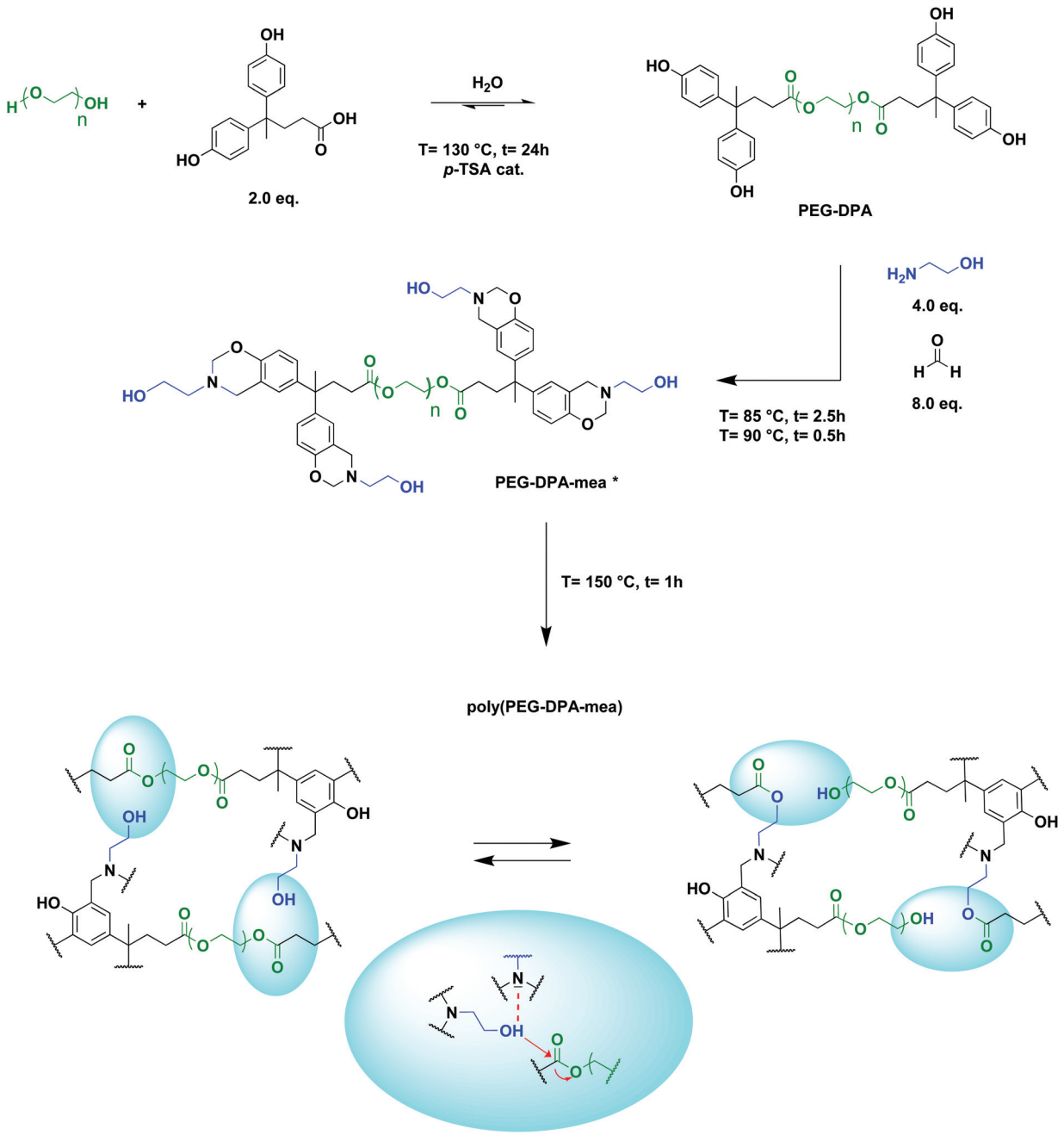

Scheme 1 Synthetic pathway to obtain poly(PEG-DPA-mea), and expected structure of the resulting vitrimer through topology rearrangement by transesterification reactions catalyzed by the *in situ* generated tertiary amines (*25% of unclosed benzoxazine rings).

previously reported in the literature.[60,61] A second exothermic peak centered around 250 °C ($T_{exo,2}$) is attributed to a thermal degradation, also confirmed by TGA (Fig. S5†). PEG_{400}-DPA-mea was subjected to a curing treatment monitored by rheology at 140 °C (Fig. 2a). The recorded rheograms present the evolution of the storage modulus (G') and the loss modulus (G'') during the polymerization of the monomer. The behavior of PEG_{400}-DPA-mea when heated is typical to thermosets with a significant increase in both G' and G''. The approximate gelation (t_{gel}), defined as the crossover point of G' and G'', was reached quickly after 145 s of isothermal curing. This high reactivity could be explained by the high functionality of the system. Rheological characterization of polymerized PEG_{400}-DPA-mea, so-called poly(PEG_{400}-DPA-mea), is reported in Fig. 2b. The measurement was done in torsion mode on a bar sample cured in a bar-shape mold as described in the Experimental section (one hour at T = 150 °C). The DSC thermogram of poly(PEG_{400}-DPA-mea) did not reveal an exothermic peak, indicating a complete polymerization (Fig. S6†). The moduli were measured to 0.6 GPa and 10 MPa in the glassy

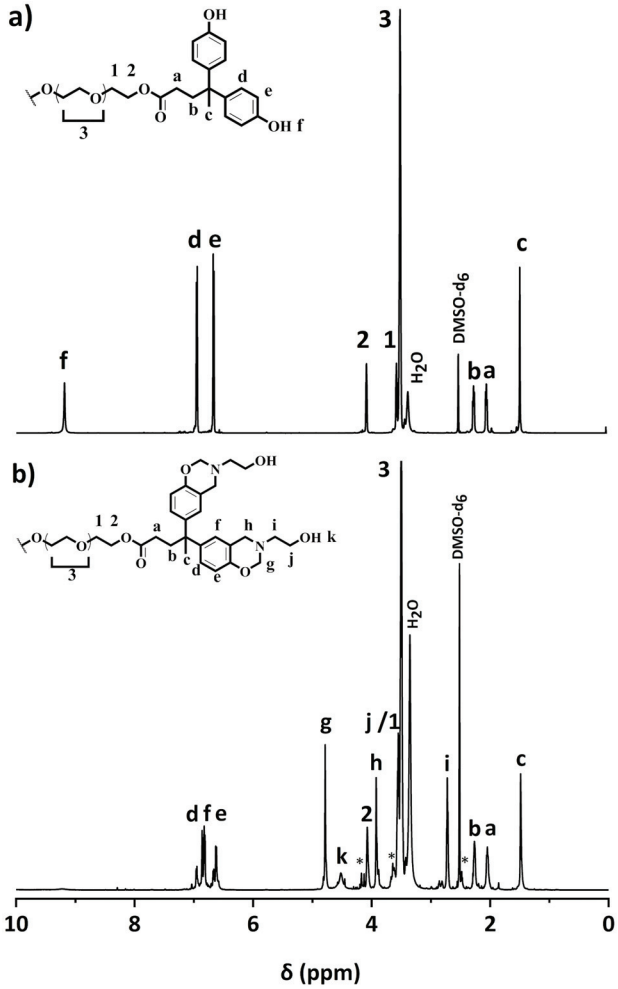

Fig. 1 ^{1}H NMR spectrum of (a) PEG_{400}-DPA and (b) PEG_{400}-DPA-mea (DMSO-d_6).

and rubbery states, respectively. The α mechanical relaxation (T_α) was measured at 93 °C according to the maximum of the tan δ. The significant broad tan delta is characteristic of networks constituted of a wide distribution of chemical structures, assigned to the transesterification reactions occurring during the curing. The T_g of poly(PEG_{400}-DPA-mea) was also measured by dilatometry (Fig. S7†). The transition was measured at the onset of the inflection (79 °C) and is more representative of the service temperature of the vitrimer than the T_α. It is worth indicating that the low thermal expansion associated to the T_g is consistent with the near-zero volumetric expansion characteristic of polybenzoxazines.[24]

3.2 Characterization of the polybenzoxazine vitrimer

3.2.1 Characterization of the vitrimer properties of poly (PEG_{400}-DPA-mea). The evolution of the relaxation modulus of poly(PEG400-DPA-mea) as a function of time and temperature (from 120 to 170 °C) shows a clear relaxation process of the modulus of poly(PEG_{400}-DPA-mea) (Fig. 3a). The relaxation time (τ^*), conventionally defined as the time for the vitrimer to relax to a value corresponding to $1/e$ (0.37) of its original modulus,[5] was measured to be 116 s at 170 °C. The temperature dependence of the relaxation time was plotted in Fig. 3b according to the Arrhenius law (5):

$$\ln\,(t^*)\,\frac{E_a}{R\times T} - \ln(A) \qquad (5)$$

The linear fitting of ln (τ^*) *versus* $1/T$ plot (correlation coefficient of 0.991) suggests that the network follows an Arrhenius-like flow characteristic. The activation energy (E_a) of transesterification reactions was obtained from the slope of the Arrhenius equation and yielded 115 kJ mol^{-1} (Fig. S7;† the detail of the calculation is reported in the ESI†). The theoretical T_v was found at 88 °C for poly(PEG_{400}-DPA-mea), in the

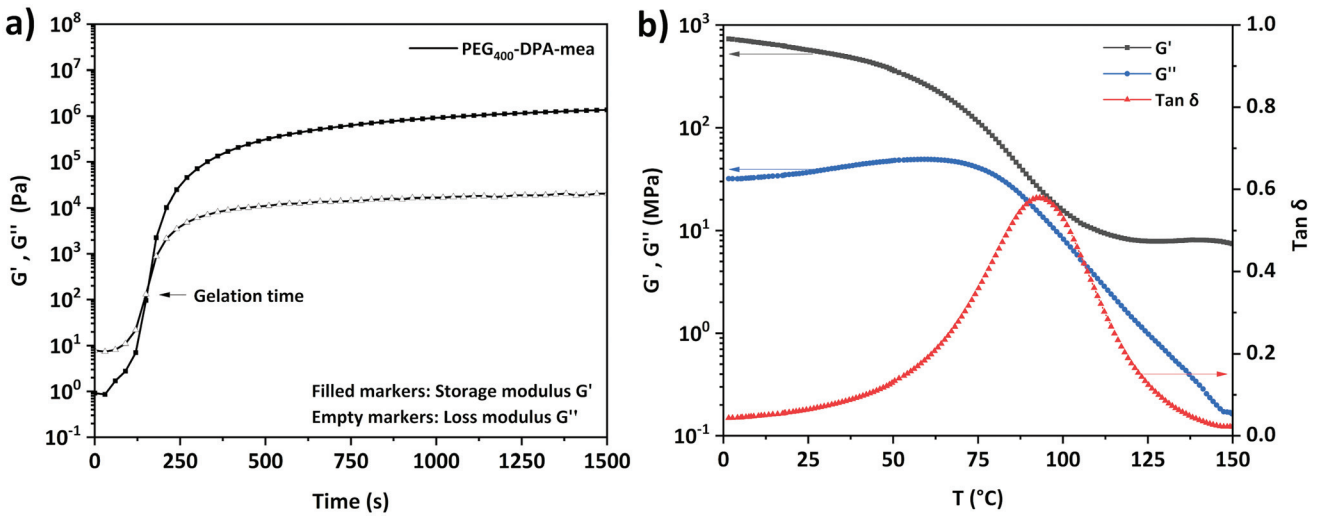

Fig. 2 (a) Isothermal rheology monitoring of PEG_{400}-DPA-mea at 140 °C (b) Rheology temperature sweep curves in torsion mode of poly(PEG_{400}-DPA-mea).

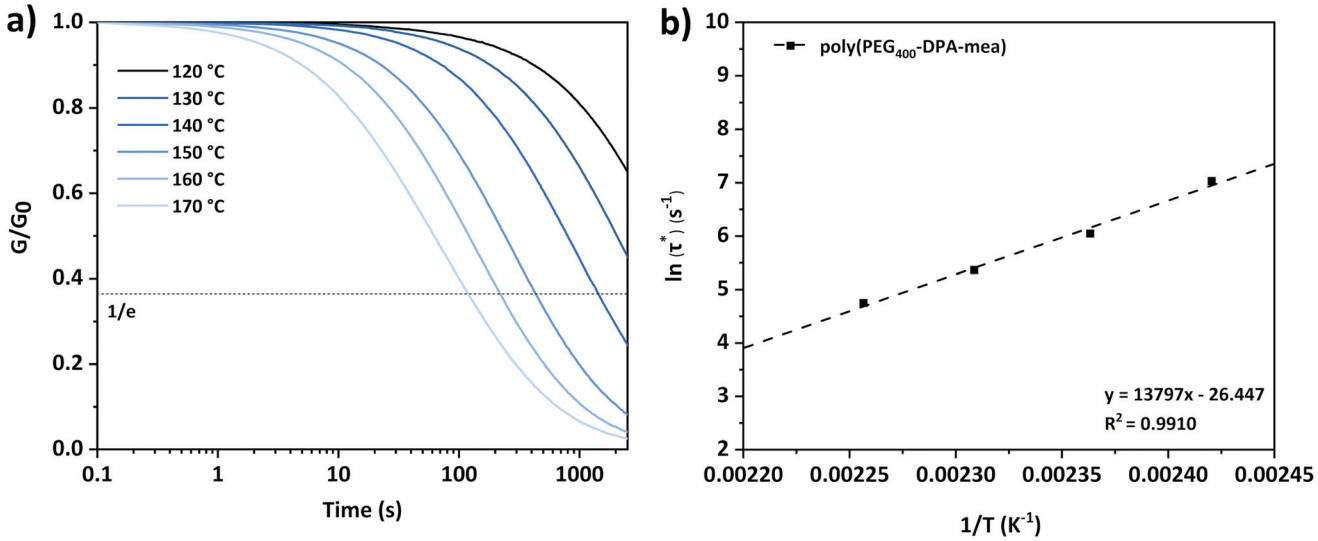

Fig. 3 (a) Stress relaxation curves of poly(PEG_{400}-DPA-mea) at different temperatures and (b) Arrhenius plot obtained from stress relaxation experiment of poly(PEG400-DPA-mea).

range of the vitrimers developed by Leibler *et al.* for epoxy/acid systems.[5,6] In the present work, the catalytic effect originates from the neighboring group participation (NGP) of the NR_3 groups in the mechanism of the TER (Scheme 1), in a similar fashion than described by Du Prez *et al.* in a recent review.[11] The activation of the –OH groups is promoted by intramolecular hydrogen bonding with the lone electron pair carried by the nitrogen atoms. While the energy of the H–O bonds decreased owing to the N–H interaction, the atom of oxygen became nucleophilic enough to attack the electrophilic center of the carbonyl bond, allowing the TER to occur.

3.2.2 Effect of the structural features on the vitrimer properties. It is generally admitted that the structural features of TER-based vitrimers are an important parameter driving their properties. The rate-enhancing effect in catalyst-free TER vitrimers is likely caused by tertiary amines and/or a high concentration of hydroxyl functions (Table 1, rows 1–7). An excess of –OH groups' was successfully used to activate ester functionalities with stress relaxation in the range of 104 s at 150 °C. (Table 1, rows 1, 3 and 4).[18–20] Later, the unique structural design of β-activated esters, more inclined to react reversibly with ester bonds due to proximity effects, was considered to elaborate vitrimers with fast stress relaxation (~1000 s at 150 °C; Table 1, row 2).[21] More recently, studies on catalyst-free vitrimers were elegantly steered toward the covalent bonding of NR_3 groups. Although the number of amines per ester bonds was quite low in each case (between 0.027 and 0.5, Table 1, rows 5–7), the TER was greatly enhanced. The concentration of exchangeable groups and the crosslinking density of the vitrimers were also described to affect lavishly the dynamicity of the crosslinked network. Dichtel *et al.* prepared a series of crosslinked polyurethane (PHU) vitrimers (derived from bis (6-membered cyclic carbonate) covering different ranges of crosslinking density.[62] According to the stress-relaxation tests, the relaxation was faster for the sample with a lower crosslinking density. They attributed this trend to the stiffness of the material and the highest chain mobility observed for the lowest crosslinking density. Abu-Omar *et al.* came to a similar conclusion for epoxy vitrimers.[63]

The effect of the structural features of the benzoxazine-based vitrimer was investigated by tuning the crosslinking density of the material and the number of –OH groups. The effect of the crosslinking density was assessed by preparing two materials with a PEG of molecular weight of either 200 or 2000 g mol^{-1}. In these materials, the ratio NR_3/ester/–OH groups (N/COO/OH) was similar (2/1/2), but the concentration of the dynamic exchangeable sites was decreasing along with the molecular weight of the PEG. Once polymerized, these materials were annotated as poly(PEG_{200}-DPA-mea) and poly (PEG_{2000}-DPA-mea) for the sake of clarity (Table 1, rows 8 and 13). The effect of the number of –OH groups was investigated by preparing three additional materials, where a part of monoethanolamine was substituted by furfurylamine (fa). They were called poly(PEG-DPA-mea_{75}/fa_{25}), poly(PEG-DPA-mea_{50}/fa_{50}), poly(PEG-DPA-mea_{25}/fa_{75}), corresponding to materials where 75%, 50% and 25% of mea was substituted by 75%, 50% and 25% of fa, respectively. NMR revealed that they correspond to materials containing a ratio of N/COO/OH equal to 2/1/1.38, 2/1/0.91 or 2/1/0.5, in respect to the order given in the sentence above (Table 1, rows 10–12). The details of the preparation and characterization of all the materials can be found in the ESI (Fig. S8–14 and S18–25†).

As expected, the crosslinking density was decreasing when the PEG molecular weight was increasing, reaching (81 ± 5) × 10^3 mol cm^{-3}, (24 ± 1) × 10^3 mol cm^{-3} and (1.5 ± 0.1) × 10^3 mol cm^{-3} for poly(PEG_{200}-DPA-mea), poly(PEG_{400}-DPA-mea) and poly(PEG_{2000}-DPA-mea) respectively. The crosslinking density of poly(PEG_{400}-DPA-mea_x/fa_{100-x}) were found to be similar to poly(PEG_{200}-DPA-mea), close to 100 × 10^3 mol cm^{-3}. They are higher than ν_e of (polyPEG_{400}-DPA-mea) in reason of

Table 1 Summary of the crosslinking density, the ratio of functionalities in self-catalyzed TER vitrimers reported in the literature and comparison of their glass transitions, relaxation times and activation energies

Network	Type of internal catalysis	$10^3 * \nu_c$ [a] (mol cm)$^{-3}$	N/COO[b]	OH/COO[d]	T_g[e] (°C)	T_α[g] (°C)	E_a[h] KJ mol^{-1})	τ^{*i} (S) [T]	Ref.
Epoxy resin	Excess of –COOH groups/β-hydroxy ester	—	—	1–2[c]	—	8	104	~10^4 [150 °C]	18
Poly(hydroxyethylmethacrylate)	β-Keto ester	2.4 ± 0.3[c]	—	1.5[c]	—	130	111	~1000 [150 °C]	21
Epoxy resin	Excess of –OH groups	—	—	>8[c]	63[f]	70	63	~4500 [180 °C]	19
Epoxy resin	Excess of –OH groups	—	—	0.625[c]	—	57	64	~5000 [180 °C]	20
Epoxy resin	Covalently bonded NR_3 groups	—	0.027 [c]	0.9[c]	—	69	94	~ 1000 [160 °C]	16
Epoxy resin	Covalently bonded NR_3 groups/β-hydroxy ester	—	0.5 [c]	1[c]	−1[f]	22	—	>10^4 [170 °C]	17
Epoxy resin	Covalently bonded NR_3 groups/excess of –OH groups	—	<0.1[c]	1[c]	120[f]	135	125	>10^4 [170 °C]	22
Polybenzoxazine	Poly(PEG_{200}-DPA-mea) Covalently bonded NR_3 groups/excess of –OH groups	81 ± 5	2	1.67*	125	—	106	814 [150 °C]	This work
	Poly(PEG_{400}-DPA-mea)	24 ± 1	2*	1.95*	79	93	115	422 [150 °C]	
	Poly(PEG_{400}-DPA-mea_{75}/fa_{25})	69 ± 1	2	1.38*	113	—	126	2012 [150 °C]	
	Poly(PEG_{400}-DPA-mea_{50}/fa_{50})	118 ± 17	2	0.91*	121	—	131	3172 [150 °C]	
	Poly(PEG_{400}-DPA-mea_{25}/fa_{75})	117 ± 19	2	0.50*	125	—	136	3410 [150 °C]	
	Poly(PEG_{2000}-DPA-mea)	1.5 ± 0.1	2	1.93*	—	−34	154	36 [150 °C]	

[a] Determined from the Flory Rehner equation (2). [b] Number of NR_3 functionalities per ester bonds (*confirmed by elemental analysis). [c] From the literature. [d] Number of –OH per ester bonds (* determined from ^{1}H NMR). [e] Determined by dilatometry experiment. [f] Determined by DSC experiment. [g] Measured from the maximum peak of tan δ curve. [h] Extrapolated from the Arrhenius equation. [i] Determined by stress relaxation experiment.

the involvement of the furan ring in the network formation.[30,41,59]

According to the stress relaxation curves, all these materials behaved like vitrimers (Tables S2–3, Fig. S15–17 and S26–29†). Their E_a and τ^* at 150 °C were determined from isothermal relaxation measurements (Table 1, column 8 and 9) and plotted in Fig. 4a and Fig. 4b as a function of their ν_c. A clear dependence of the Ea on the number of –OH groups is depicted on Fig. 4a (values encircled by a dashed line). Despite their similar crosslinking density, the E_a of poly(PEG-DPA-mea_{75}/fa_{25}), poly(PEG-DPA-mea_{50}/fa_{50}), and poly(PEG-DPA-mea_{25}/fa_{75}) are increasing while the amount of –OH groups is decreasing (E_a = 126, 131, 136 kJ mol^{-1} respectively). In the case of poly(PEG_{2000}-DPA-mea), which crosslinking density is the lowest, E_a reached the value of 156 kJ mol^{-1}. In the more crosslinked network (poly(PEG_{200}-DPA-mea)), E_a decreased to 106 kJ mol^{-1}. Lowering the concentration of –OH groups, either by decreasing the ν_c or the total amount of –OH groups leads to an increase of the E_a. These experiments confirm that the energy needed to activate the dynamic exchanges is clearly governed both by the excess of –OH groups and the concentration of dynamic sites in the network. It is worth indicating the E_a related to the relaxation of theses PBZs vitrimer are in the same range than other reported vitrimers catalyzed either by external or internal tertiary amine.[5,6,16,22] However it cannot be excluded that aromatic –OH groups may also be involved in the transesterification mechanism and contribute to the high value of E_a. Indeed, the transesterification with phenoxy is well documented.[64–66] Nevertheless, it is worthy to mention that even after a couple of hours at 170 °C, the relaxation of PEG_{400}-DPA-fa, *i.e.* in the absence of aliphatic –OH was not observed. The results do not exclude the possible involvement of the phenoxy groups in the exchanges, but it is not observed in the conditions of the experiments described here.

The evolution of τ^* follows another trend (Fig. 4b). A clear dependence exists with the concentration of –OH groups, as attested by the significant increase of τ^* when decreasing the amount of –OH groups for materials of similar ν_c (poly(PEG_{400}-DPA-mea_x/fa_{100-x})). τ^* remains reasonable (lower than 1 hour at 150 °C) even for the material displaying the lower amount of –OH groups (Table 1, row 12). However, despite their lowest concentration of dynamic sites, the fastest behaviors were reached for the materials with the lowest ν_c (Table 1, rows 9 and 13). This trend indicates that the speed of the dynamic exchange is also driven by the mobility of the chains.[62,63]

The very short τ^* compared to similar catalyst-free vitrimers can be explained by the abundant number of NR_3 groups (coming from the benzoxazine ROP). Indeed, the polymerization of PEG_n-DPA-mea_x/fa_{100-x} follows a ROP, which leads to the formation of a network with an abundant number of tertiary amines, significantly higher in comparison to the previously reported catalyst-free vitrimers (Table 1, column 4). Therefore, the nucleophile substitution of the ester bonds by

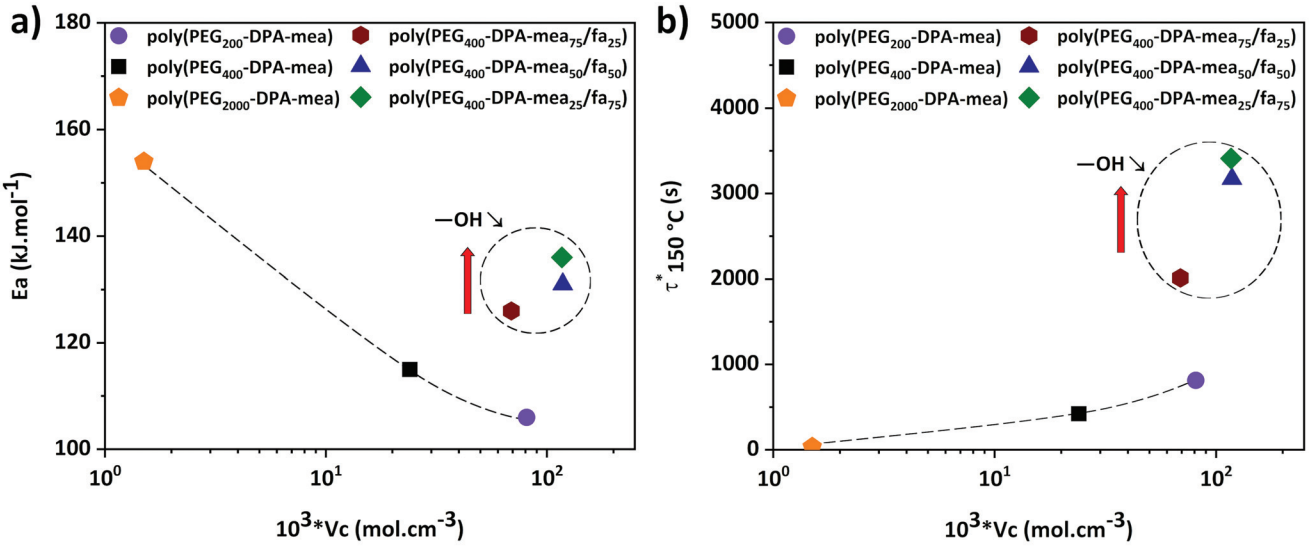

Fig. 4 Evolution of $\tau^*_{150°C}$ and E_a as a function of the crosslinking density of the different polybenzoxazine vitrimer.

the –OH groups is highly promoted. This behavior is in adequation with one of the first observations made by Leibler *et al.* about the relationship between the amount of catalyst and the short τ^* of vitrimers.[6] Moreover, the catalytic effect is more pronounced thanks to the close position of the NR_3 groups regarding the –OH groups, in agreement with the NGP theory recently disclosed by Du Prez *et al.*[11] and illustrated in Scheme 1.

3.3 Self-healing, recycling, reprocessing and reshaping

Additional swelling experiments were performed in different solvents for poly(PEG_{400}-DPA-mea). The material is insoluble

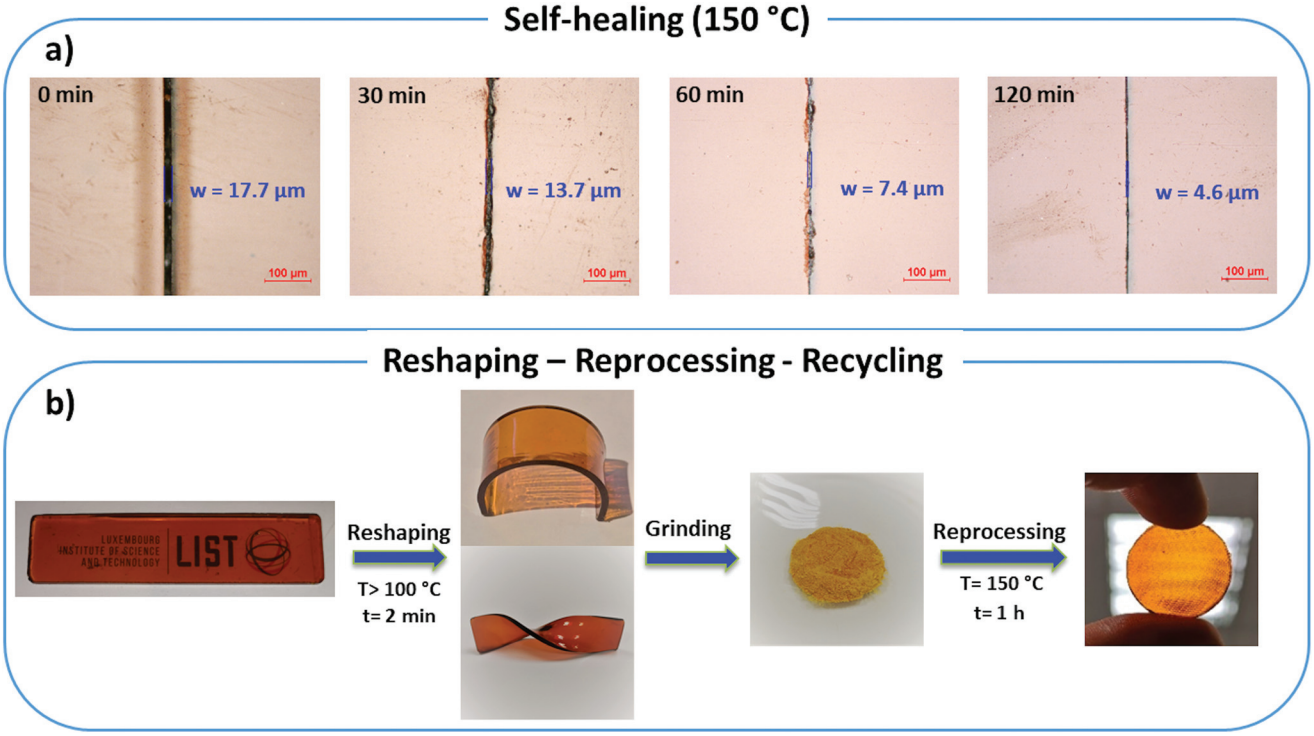

Fig. 5 (a) Self-healing behavior of poly(PEG_{400}-DPA-mea) (b) Life cycle of the bio-based polybenzoxazine vitrimer by reshaping, reprocessing and recycling.

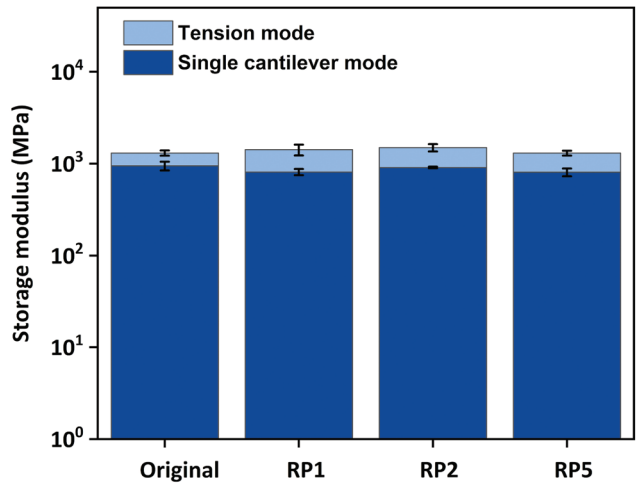

Fig. 6 Storage modulus of poly(PEG_{400}-DPA-mea) determined in tensile and single cantilever mode after successive recycling (one, two and five times respectively).

in acetone, water, and chloroform, in which it swells by 14%, 38%, and 103% respectively after 24 hours (Fig. S30†). Later, the samples were dried and weighted to determine the soluble part, measured to be lower than 5 wt%. The chemical recyclability of poly(PEG_{400}-DPA-mea) was illustrated by its chemical decomposition in acetic acid at RT (Fig. S31†). The self-healability of poly(PEG_{400}-DPA-mea) was demonstrated by surface morphology analysis recorded by optical microscopy (Fig. 5a). The cured material was notched with a scalpel blade, forming a scratch of 17.7 μm initial width. When exposed at 150 °C in pressure-free conditions, the width of the damaged area gradually decreased with time, reaching 4.6 μm (*i.e.* less than 25% of the initial scratch width) after 120 min. The reshaping, twisting and bending of materials made of poly(PEG_{400}-DPA-mea) were straightforward, thanks to the fast relaxation process (Fig. 5b). The reprocessability was investigated by grinding the material into a fine powder, after which it was compressed to the shape of either a disk or a bar. The reprocessed bar was then subjected to dynamic mechanical tests in tensile and single cantilever modes to determine the impact of the reprocessing on their mechanical properties (Fig. 6). The storage modulus (E') of poly(PEG_{400}-DPA-mea) (1307 ± 86 MPa) was fully recovered even after being ground and reshaped five times (1306 ± 81 MPa). Besides storing the mechanical properties, the overlap of the FTIR spectra of both cured and reprocessed materials provides evidence that poly(PEG_{400}-DPA-mea) did not show any deterioration of its chemical structure after 5 recycling steps (Fig. S32†).

Conclusions

This study relates the synthesis and the properties of a catalyst-free and bio-based polybenzoxazine vitrimer. The synthesis pathway consisted of a solventless two-step reaction, including the Fischer esterification of 4,4-bis(4-hydroxyphenyl) valeric acid and polyethylene glycol, which was then reacted with mono-ethanolamine and paraformaldehyde *via* a Mannich-like condensation. Quadri-telechelic benzoxazine-terminated polyethylene glycol monomers containing ester bonds and pendant aliphatic hydroxyl groups (PEG_{400}-DPA-mea) were obtained. The chemical structure of the monomers was confirmed by ^{1}H NMR, ^{13}C NMR, elemental analysis, and FTIR. The vitrimer (poly(PEG_{400}-DPA-mea)) was formed by triggering the ring-opening polymerization of the benzoxazine moieties at 150 °C for one hour, leading to a covalently bonded network with an abundant number of tertiary amines per ester bond. The mechanical properties of the resulting PBz were assessed by rheological characterization. The achievement of a cross-linked structure was attested by the ability of the material to swell in common organic solvents, with a soluble fraction lower than 5 wt%. Due to the ability of tertiary nitrogen groups to catalyze transesterification reactions, the material enabled fast exchange reactions without the use of an external catalyst, as attested by short stress-relaxation times (116 s at 170 °C). The activation energy of the ester bond exchange was found to be 115 kJ mol^{-1}, in the range of transesterification reactions catalyzed by tertiary amines. The effect of the structural features of the vitrimer was also investigated by tuning the cross-linking density of the network and the amount of –OH groups. It showed that the energy needed to activate the dynamic exchanges is clearly governed both by the excess of –OH groups and the concentration of dynamic sites in the network. The very short relaxation times were explained by the neighboring group participation theory, the abundant number of tertiary N groups and the flexibility of the network.

The self-healing, recycling, reshaping, and reprocessing of poly(PEG_{400}-DPA-mea) without any loss of properties were successfully demonstrated. Therefore, this research reflects the suitability of polybenzoxazines to design easily synthesizable mono-component, catalyst-free, and fast responsive vitrimers.

Abbreviations

CAN	Covalent adaptable network
DCB	Dynamic covalent bond
TER	Transesterification reaction
–OH	Aliphatic hydroxyl
$Zn(OAc)_2$	Zinc acetate
NR3	Tertiary amine
TBD	Triazobicyclodecene
PBZs	Polybenzoxazines
ROP	Ring-opening polymerization
PFA	Paraformaldehyde
DPA	Diphenolic acid
PEG	Polyethylene glycol
PEG-DPA	Quadri-telechelic phenol-terminated PEG
mea	Mono-ethanolamine

PEG-DPA-mea	Quadri-telechelic benzoxazine-terminated polyethylene glycol monomer
fa	Furfurylamine
p-TSA	*para*-Toluene sulfonic acid
NMR	Nuclear magnetic resonance
TMS	Tetramethylsilane
FTIR	Fourier transform infrared spectroscopy
ATR	Attenuated total reflection
N_2	Nitrogen
$T_{desorpt.}$	Desorption temperature
TCD	Thermal conductivity detector
DSC	Differential scanning calorimetry
T_g	Glass transition
TGA	Thermogravimetric analysis
DTG	Derivative tthermogravimetric Analysis
DMA	Dynamic mechanical analysis
RT	Room temperature
G_0	Original relaxation modulus
G'/E'	Storage modulus
G''	Loss modulus
W	Swelling ratio
$\overline{M_c}$	Molecular weight between crosslinks
ν_c	Crosslinking density
DMSO-d_6	Deuterated dimethylsulfoxide
Poly(PEG-DPA-mea)	Polymerized PEG-DPA-mea
PEG_n	Polyethylene glycol of molecular weight n (g mol^{-1})
Tan δ	Loss factor
τ^*	Relaxation time
E_a	Activation energy
NGP	Neighboring group participation

Author contributions

Antoine Adjaoud: validation, investigation, writing – original draft, writing – review and editing. Acerina Trejo-Machin: validation, investigation, writing – review and editing. Laura Puchot: validation, investigation, writing – original draft, writing – review and editing. Pierre Verge: conceptualization, validation, investigation, resources, writing – original draft, writing – review and editing, supervision, project administration.

Funding sources

This research was supported by the Luxembourg National Research Fund (FNR), Grant number: C18/MS/12538602.

Conflicts of interest

There are no conflicts of interest to declare.

Acknowledgements

The authors would like to thank the FNR for the funding of the project LIGNOBENZ (C18/MS/12538602). The authors are also extremely thankful to Benoit Marcolini, Régis Vaudemont, Lindsey Auguin, and Denis Pittois. The authors would also like to thank Laurent Sabatie and Dr Daniel Schmidt for the intellectual and technical discussions related to vitrimers.

Notes and references

1 K. L. Forsdyke and T. F. Starr, *Thermoset Resins*, iSmithers Rapra Publishing, 2002.
2 S. J. Rowan, S. J. Cantrill, G. R. L. Cousins, J. K. M. Sanders and J. F. Stoddart, *Angew. Chem., Int. Ed.*, 2002, **41**, 898–952.
3 S. D. Bergman and F. Wudl, *J. Mater. Chem.*, 2008, **18**, 41–62.
4 C. J. Kloxin, T. F. Scott, B. J. Adzima and C. N. Bowman, *Macromolecules*, 2010, **43**, 2643–2653.
5 D. Montarnal, M. Capelot, F. Tournilhac and L. Leibler, *Science*, 2011, **334**, 965–968.
6 M. Capelot, M. M. Unterlass, F. Tournilhac and L. Leibler, *ACS Macro Lett.*, 2012, **1**, 789–792.
7 M. Capelot, D. Montarnal, F. Tournilhac and L. Leibler, *J. Am. Chem. Soc.*, 2012, **134**, 7664–7667.
8 W. Denissen, J. Winne and F. Du Prez, *Chem. Sci.*, 2015, **7**, 30–38.
9 J. Winne, L. Leibler and F. Du Prez, *Polym. Chem.*, 2019, **10**, 6091–6108.
10 M. Guerre, C. Taplan, J. M. Winne and F. E. Du Prez, *Chem. Sci.*, 2020, **11**, 4855–4870.
11 F. Van Lijsebetten, J. O. Holloway, J. M. Winne and F. E. Du Prez, *Chem. Soc. Rev.*, 2020, **49**, 8425–8438.
12 D. J. Fortman, J. P. Brutman, G. X. De Hoe, R. L. Snyder, W. R. Dichtel and M. A. Hillmyer, *ACS Sustainable Chem. Eng.*, 2018, **6**, 11145–11159.
13 J. Otera, *Chem. Rev.*, 1993, **93**, 1449–1470.
14 U. Schuchardt, R. Sercheli and V. Matheus, *J. Braz. Chem. Soc.*, 1998, **9**, 199–210.
15 M. K. Kiesewetter, M. D. Scholten, N. Kirn, R. L. Weber, J. L. Hedrick and R. M. Waymouth, *J. Org. Chem.*, 2009, **74**, 9490–9496.
16 F. I. Altuna, C. E. Hoppe and R. J. J. Williams, *Eur. Polym. J.*, 2019, **113**, 297–304.
17 Y. Li, T. Liu, S. Zhang, L. Shao, M. Fei, H. Yu and J. Zhang, *Green Chem.*, 2020, **22**, 870–881.
18 F. I. Altuna, V. Pettarin and R. J. J. Williams, *Green Chem.*, 2013, **15**, 3360–3366.
19 J. Han, T. Liu, C. Hao, S. Zhang, B. Guo and J. Zhang, *Macromolecules*, 2018, **51**, 6789–6799.
20 T. Liu, S. Zhang, C. Hao, C. Verdi, W. Liu, H. Liu and J. Zhang, *Macromol. Rapid Commun.*, 2019, **40**, 1800889.
21 S. Debnath, S. Kaushal and U. Ojha, *ACS Appl. Polym. Mater.*, 2020, **2**, 1006–1013.

22 C. Hao, T. Liu, S. Zhang, W. Liu, Y. Shan and J. Zhang, *Macromolecules*, 2020, **53**, 3110–3118.
23 X. Ning and H. Ishida, *J. Polym. Sci., Part A: Polym. Chem.*, 1994, **32**, 1121–1129.
24 H. Ishida, in *Handbook of Benzoxazine Resins*, ed. H. Ishida and T. Agag, Elsevier, Amsterdam, 2011, pp. 3–81.
25 E. Calò, A. Maffezzoli, G. Mele, F. Martina, S. E. Mazzetto, A. Tarzia and C. Stifani, *Green Chem.*, 2007, **9**, 754–759.
26 N. N. Ghosh, B. Kiskan and Y. Yagci, *Prog. Polym. Sci.*, 2007, **32**, 1344–1391.
27 M. Comí, G. Lligadas, J. C. Ronda, M. Galià and V. Cádiz, *J. Polym. Sci., Part A: Polym. Chem.*, 2013, **51**, 4894–4903.
28 L. Dumas, L. Bonnaud, M. Olivier, M. Poorteman and P. Dubois, *J. Mater. Chem. A*, 2015, **3**, 6012–6018.
29 L. Puchot, P. Verge, T. Fouquet, C. Vancaeyzeele, F. Vidal and Y. Habibi, *Green Chem.*, 2016, **18**, 3346–3353.
30 C. Wang, J. Sun, X. Liu, A. Sudo and T. Endo, *Green Chem.*, 2012, **14**, 2799–2806.
31 N. K. Sini, J. Bijwe and I. K. Varma, *J. Polym. Sci., Part A: Polym. Chem.*, 2014, **52**, 7–11.
32 P. Thirukumaran, A. Shakila Parveen and M. Sarojadevi, *ACS Sustainable Chem. Eng.*, 2014, **2**, 2790–2801.
33 P. Froimowicz, C. R. Arza, L. Han and H. Ishida, *ChemSusChem*, 2016, **9**, 1921–1928.
34 L. Dumas, L. Bonnaud, M. Olivier, M. Poorteman and P. Dubois, *Green Chem.*, 2016, **18**, 4954–4960.
35 X. Liu, R. Zhang, T. Li, P. Zhu and Q. Zhuang, *ACS Sustainable Chem. Eng.*, 2017, **5**, 10682–10692.
36 B. Kiskan, *React. Funct. Polym.*, 2018, **129**, 76–88.
37 M. L. Salum, D. Iguchi, C. R. Arza, L. Han, H. Ishida and P. Froimowicz, *ACS Sustainable Chem. Eng.*, 2018, **6**, 13096–13106.
38 L. Bonnaud, B. Chollet, L. Dumas, A. A. M. Peru, A. L. Flourat, F. Allais and P. Dubois, *Macromol. Chem. Phys.*, 2019, **220**, 1800312.
39 N. Amarnath, S. Shukla and B. Lochab, *ACS Sustainable Chem. Eng.*, 2018, **6**, 15151–15161.
40 M. Monisha, N. Amarnath, S. Mukherjee and B. Lochab, *Macromol. Chem. Phys.*, 2019, **220**, 1970005.
41 S. Ren, X. Miao, W. Zhao, S. Zhang and W. Wang, *Mater. Today Commun.*, 2019, **20**, 100568.
42 Y. Lyu and H. Ishida, *Prog. Polym. Sci.*, 2019, **99**, 101168.
43 N. Amarnath, S. Shukla and B. Lochab, *ACS Sustainable Chem. Eng.*, 2019, **7**, 18700–18710.
44 L. E. Heim, H. Konnerth and M. H. G. Prechtl, *Green Chem.*, 2017, **19**, 2347–2355.
45 R. Tavernier, L. Granado, G. Foyer, G. David and S. Caillol, *Macromolecules*, 2020, **53**, 2557–2567.
46 R. Tavernier, L. Granado, G. Foyer, G. David and S. Caillol, *Polymer*, 2020, 123270.
47 O. S. Taskin, B. Kiskan and Y. Yagci, *Macromolecules*, 2013, **46**, 8773–8778.
48 M. Arslan, B. Kiskan and Y. Yagci, *Macromolecules*, 2015, **48**, 1329–1334.
49 M. Arslan, B. Kiskan and Y. Yagci, *Macromolecules*, 2018, **51**, 10095–10103.
50 A. Trejo-Machin, L. Puchot and P. Verge, *Polym. Chem.*, 2020, **11**, 7026–7034.
51 A. Trejo-Machin, P. Verge, L. Puchot and R. Quintana, *Green Chem.*, 2017, **19**, 5065–5073.
52 J. J. Bozell, L. Moens, D. C. Elliott, Y. Wang, G. G. Neuenscwander, S. W. Fitzpatrick, R. J. Bilski and J. L. Jarnefeld, *Resour., Conserv. Recycl.*, 2000, **28**, 227–239.
53 V. Froidevaux, C. Negrell, S. Caillol, J.-P. Pascault and B. Boutevin, *Chem. Rev.*, 2016, **116**, 14181–14224.
54 M. Pelckmans, T. Renders, S. Van de Vyver and B. F. Sels, *Green Chem.*, 2017, **19**, 5303–5331.
55 C. Özdemir and A. Güner, *J. Appl. Polym. Sci.*, 2006, **101**, 203–216.
56 J. Chen, S. K. Spear, J. G. Huddleston and R. D. Rogers, *Green Chem.*, 2005, **7**, 64–82.
57 H. A. Bruson, *J. Am. Chem. Soc.*, 1936, **58**, 1741–1744.
58 N. G. Kandile, T. M. A. Razek, A. M. Al-Sabagh and M. M. T. Khattab, *Egypt. J. Pet.*, 2014, **23**, 323–329.
59 A. Trejo-Machin, A. Adjaoud, L. Puchot, R. Dieden and P. Verge, *Eur. Polym. J.*, 2020, **124**, 109468.
60 B. Kiskan, B. Koz and Y. Yagci, *J. Polym. Sci., Part A: Polym. Chem.*, 2009, **47**, 6955–6961.
61 R. Kudoh, A. Sudo and T. Endo, *Macromolecules*, 2010, **43**, 1185–1187.
62 D. J. Fortman, J. P. Brutman, M. A. Hillmyer and W. R. Dichtel, *J. Appl. Polym. Sci.*, 2017, **134**, 44984.
63 S. Zhao and M. M. Abu-Omar, *Macromolecules*, 2019, **52**, 3646–3654.
64 R. S. Porter and L.-H. Wang, *Polymer*, 1992, **33**, 2019–2030.
65 Y. Yuan and E. Ruckenstein, *Polymer*, 1998, **39**, 1893–1897.
66 P. Baumhof, R. Mazitschek and A. Giannis, *Angew. Chem., Int. Ed.*, 2001, **40**, 3672–3674.